A Statistical Theory of Homogeneous Isotropic Turbulence

Nicola de Divitiis*

Department of Mechanics and Aeronautics

University "La Sapienza", Rome, Italy

(Dated: February 11, 2009)

Abstract

The present work proposes a theory of isotropic and homogeneous turbulence for incompressible fluids, which assumes that the turbulence is due to the bifurcations associated to the velocity field. The theory is formulated using a representation of the fluid motion which is more general than the classical Navier-Stokes equations, where the fluid state variables are expressed in terms of the referential coordinates.

The theory is developed according to the following four items: 1) Study of the route toward the turbulence through the bifurcations analysis of the kinematic equations. 2) Referential description of the motion and calculation of the velocity fluctuation using the Lyapunov analysis of the local deformation. 3) Study of the mechanism of the energy cascade from large to small scales through the Lyapunov analysis of the relative kinematics equations of motion. 4) Determination of the statistics of the velocity difference with the Fourier analysis. Each item contributes to the formulation of the theory.

The theory gives the connection between number of bifurcations, scales and Reynolds number at the onset of the turbulence and supplies an explanation for the mechanism of the energy cascade which leads to the closure of the von Kármán-Howarth equation. The theory also gives the statistics of the velocity difference fluctuation and permits the calculation of its PDF.

The presented results show that the proposed theory describes quite well the properties of the isotropic turbulence.

PACS numbers: Valid PACS appear here

*via Eudossiana, 18, 00184, Rome; Electronic address: dedivitiis@dma.dma.uniroma1.it

I. INTRODUCTION

This work presents a theory of isotropic and homogeneous turbulence for an incompressible fluid formulated for an infinite fluid domain. The theory is mainly motivated by the fact that in turbulence the fluid kinematics is subjected to bifurcations [1] and exhibits a chaotic behavior and huge mixing [2], resulting to be much more rapid than the fluid state variables. This characteristics implies that the accepted kinematical hypothesis for deriving the Navier-Stokes equations could require the consideration of very small length scales and times for describing the fluid motion [3] and therefore a very large number of degrees of freedom. To avoid the difficulties arising from the consideration of these small scales, the referential description of motion is adopted, where the fluid state variables are expressed in terms of the so called referential coordinates which coincide with the material coordinates for a given fluid configuration [3].
The other very important subjects of the turbulence are the non-gaussian statistics of the velocity difference and the mechanism of the kinetic energy cascade. This latter is directly related to the relative motion of a pair of fluid particles [4, 5, 6, 7] and is responsible for the shape of the developed energy spectrum.

For these reasons the present theory is based on:

1. Landau hypothesis, following which the turbulence is caused by the bifurcations of the velocity field [1].

2. Referential description of motion, where velocity field and stress tensor are mapped with respect to the referential coordinates [3].

3. Study of the energy cascade through Lyapunov analysis of the relative kinematics.

4. Statistical analysis of the velocity difference fluctuations.

In the first part of the work, the road toward the turbulence is studied through the bifurcations analysis of the kinematic equations. These bifurcations arise from the mathematical structure of the velocity field, where the Reynolds number plays the role of the "control parameter". This analysis supplies the connection between number of bifurcations and the critical Reynolds number for isotropic turbulence, showing that the length scales

are continuously distributed and that each of them is important for the description of the motion.

In the second part, the momentum equations are formulated according to the referential representation of motion, whereas the kinematics of the local deformation is studied with the Lyapunov theory. The fluid motion is described adopting the referential configuration which corresponds to the fluid placement at the onset of this fluctuation. This choice allows the velocity fluctuations to be analytically expressed through the Lyapunov analysis of the kinematics of the fluid deformation.

The third part deals with the relative kinematic between two trajectories, which is also analyzed with the Lyapunov theory. This analysis gives an explanation of the mechanism of kinetic energy transfer between length scales and leads to the closure of the von Kármán-Howarth equation [6] (see Appendix), where the unknown function $K(r)$, which represents the inertia forces, is here expressed in terms of the longitudinal correlation function. The obtained expression of $K(r)$ satisfies the conservation law which states that the inertia forces only transfer the kinetic energy [6, 7].

To complete the theory, the statistics of velocity difference is studied through the Fourier analysis of the velocity fluctuations. An analytical expression for the velocity difference and for its PDF is obtained in case of isotropic turbulence. This expression incorporates an unknown function, related to the skewness, which is immediately identified through the obtained expression of $K(r)$.

Finally, the several results obtained with this theory are compared with the data existing in the literature, indicating that the proposed theory adequately describes the various properties of the turbulence.

II. BIFURCATION ANALYSIS OF THE KINEMATIC EQUATIONS

In this session, the route toward the turbulence is studied through the analysis of the bifurcations of the kinematic equations. To analyze this question, a viscous and incompressible fluid in the infinite domain is considered, whose kinematic equations are

$$\frac{d\mathbf{x}}{dt} = \mathbf{u}(\mathbf{x}, t; Re) \tag{1}$$

where $\mathbf{x}$ and Re are the position and Reynolds number, whereas $\mathbf{u}(\mathbf{x}, t; Re)$ is a single realization of the ensemble of the velocity fields, written in the reference frame $\Re$, which satisfies the Navier-Stokes equations

$$\begin{aligned} \nabla \cdot \mathbf{u} &= 0 \\ \frac{\partial \mathbf{u}}{\partial t} + \mathbf{u}\nabla\mathbf{u} + \frac{\nabla p}{\rho} - \nu\nabla^2\mathbf{u} &= 0 \end{aligned} \tag{2}$$

ρ and ν are, respectively, density and kinematic viscosity whereas p is the fluid pressure which can be eliminated by taking the divergence of the momentum equation [7]

$$\frac{\nabla^2 p}{\rho} + \nabla\mathbf{u} : \nabla\mathbf{u} = 0 \tag{3}$$

Now, let consider an assigned velocity field at a given time, and the fixed points $\mathbf{X}$ of Eq. (1) which satisfy to $d\mathbf{X}/dt = 0$. Increasing the Reynolds number, $\mathbf{X}$ will vary according to Eq. (1), which can be solved by the continuation method [8, 9]

$$\mathbf{X} = \mathbf{X}_0 - \int_{Re_0}^{Re} \nabla\mathbf{u}^{-1} \frac{\partial \mathbf{u}}{\partial Re}\, dRe \tag{4}$$

where $\mathbf{X}_0$ is the fixed point calculated at $Re = Re_0$. The Reynolds number influences the mathematical structure of Eq. (1) through the Navier-Stokes equations in such a way that, for small Re, the viscosity forces which are stronger than the inertia ones, make $\mathbf{u}$ an almost

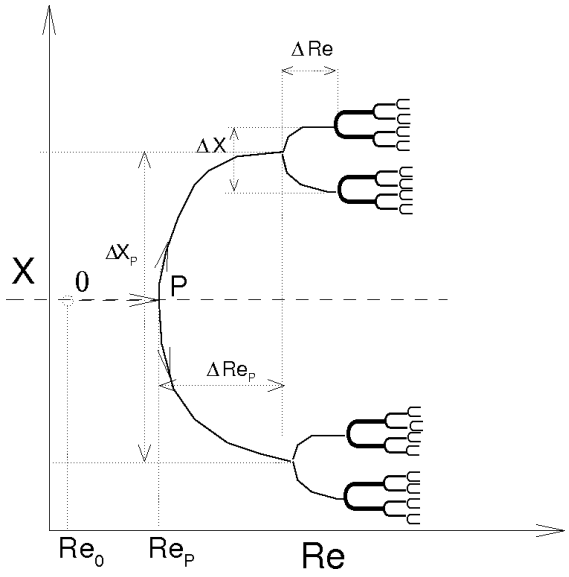

FIG. 1: Map of the bifurcations.

smooth function of $\mathbf{X}$. When the Reynolds number increases, as long as the Jacobian $\nabla\mathbf{u}$ is nonsingular, $\mathbf{X}$ exhibits smooth variations with Re, whereas at a certain Re, this Jacobian becomes singular due to the higher inertia-viscous forces ratio, resulting $\det(\nabla\mathbf{u}) = 0$. This can correspond to the first bifurcation, where at least one of the eigenvalues of $\nabla\mathbf{u}$ crosses the imaginary axis and $\mathbf{X}$ appears to be discontinuous with respect to Re [8, 9]. Increasing again the Reynolds number, $\mathbf{X}$ will show smooth variations until to the next bifurcation.

Figure 1 shows a scheme of bifurcations, where the component X of $\mathbf{X}$ is reported in terms of Reynolds number. Starting from Re_0, the diagram is regular, until to Re_P, where the first bifurcation determines two branches, whose distance ΔX_P is measured at the next bifurcation. For each bifurcation, ΔX gives a length scale of the velocity field at the current Reynolds number, whereas ΔRe represents the distance between two successive bifurcations. After P, Eq. (4) does not indicate which of the two possible branches the system will choose, thus a bifurcation causes a lost of informations with respect to the initial data [10]. Therefore, the fluctuations are important for the choice of the branch that the system will follow [10].

Further increments of Re cause an increment of the number of bifurcations whose scaling laws are described by the two successions [9, 11]

$$\alpha_n = \frac{\Delta X_n}{\Delta X_{n+1}}, \quad \delta_n = \frac{\Delta Re_n}{\Delta Re_{n+1}} \tag{5}$$

For $Re \to \infty$, the convergence of α_n and δ_n is not granted in general, whereas for period-doubling bifurcations, these admit the following limits [11]

$$\alpha = \lim_{Re\to\infty} |\alpha_n| = 2.502... \quad \delta = \lim_{Re\to\infty} |\delta_n| = 4.669... \tag{6}$$

These are the famous Feigenbaum numbers, which are two universal constants, independent on the mathematical details of the period-doubling bifurcations. For bifurcations of other kind, α_n and δ_n can converge to different values or can oscillate around to average values.

In the present analysis, the length scales $l_n \equiv \Delta X_n$ are assumed to be expressed by the asymptotic approximation

$$l_n = \frac{l_1}{\alpha^{n-1}} \tag{7}$$

Equation (7) supplies the length scales in terms of the numbers of the bifurcations encountered along a given path of fixed points, where α is the Feigenbaum constant given by Eq. (6) and l_1 represents the maximum length scale. According to [11, 12, 13, 14], the bifurcations

generate a route toward the chaos which depends on n. As long as $n \leq 2$, each bifurcation adds a new frequency into the power spectrum of $\mathbf{u}$ and this corresponds to limit cycles or quasi periodic motions, whereas for $n \geq 3$, the situation drastically changes, since $\mathbf{u}$ exhibits more numerous frequencies and this generates chaotic motion [11, 12]. This occurs for a single realization of the ensemble of the velocity field. The fluctuations of $\mathbf{u}(\mathbf{x}, t)$ will cause further variations of the several scales l_n in Eq. (7), thus the bifurcations maps will be more complicated than Fig. 1, and the recognizing the diverse scales and bifurcations could not be possible. This is a scenario with continuously distributed length scales, where all of them are important for describing the fluid motion.

A. Critical Reynolds number

Equation (7) describes the route toward the chaos and is assumed to be valid until the onset of the turbulence. In this situation the minimum for l_n can not be less than the dissipation length or Kolmogorov scale $\ell = (\nu^3/\varepsilon)^{1/4}$ [1], where ε is the energy dissipation rate (see Appendix), whereas l_1 gives a good estimation of the correlation length of the phenomenon [8, 10] which, in this case is the Taylor scale λ_T. Thus, $\ell < l_n < \lambda_T$, and

$$\ell = \frac{\lambda_T}{\alpha^{N-1}} \tag{8}$$

where N is the number of bifurcations at the beginning of the turbulence.

Equation (8) gives the connection between the critical Reynolds number and number of bifurcations. In fact, the characteristic Reynolds numbers associated to the scales ℓ and λ_T are $R_K = \ell u_K/\nu \equiv 1$ and $R_\lambda = \lambda_T u/\nu$, respectively, where $u_K = (\nu\varepsilon)^{1/4}$ is characteristic velocity at the Kolmogorov scale, and $u = \sqrt{\langle u_i u_i \rangle /3}$ is the velocity standard deviation [7]. For isotropic turbulence, these scales are linked each other by [7]

$$\lambda_T/\ell = 15^{1/4}\sqrt{R_\lambda} \tag{9}$$

In view of Eq.(8), this ratio can be also expressed through N.

$$\alpha^{N-1} = 15^{1/4}\sqrt{R_\lambda} \tag{10}$$

The value $R_\lambda \simeq 1.613$ obtained for $N = 2$ is not compatible with λ_T which is the correlation scale, while the result $R_\lambda \simeq 10.12$, calculated for $N = 3$, is an acceptable minimum value

for R_λ. This result agrees with the various scenarios describing the roads to the turbulence [11, 12, 13, 14], and with the diverse experiments [15, 16, 17] which state that the turbulence begins for $N \geq 3$. Of course, this minimum value for R_λ is the result of the assumptions $\alpha \simeq 2.502$, $l_1 \simeq \lambda_T$, $l_N \simeq \ell$ and of the asymptotic approximation (7).

III. REFERENTIAL DESCRIPTION OF MOTION. VELOCITY FLUCTUATION

Now, we present a formulation of the fluid equations of motion which is based on the referential description of the motion. This formulation is more general than the classical Navier-Stokes equations and is capable to take into account the effects of the fluid kinematics which can be much faster than the fluid state variables. This description of motion allows to calculate the velocity fluctuation through the Lyapunov analysis of the local deformation.

This representation of motion is based on the fact that a given fluid property Ω is an explicit function of the referential displacement $\mathbf{x}_0$ and of the time [3], i.e.

$$\Omega = \Omega(\mathbf{x}_0, t) \tag{11}$$

The referential displacement coincides with the material position for a given fluid configuration, thus $\mathbf{x}_0$ plays the role of the label which identifies the specific fluid particle [3]. Since

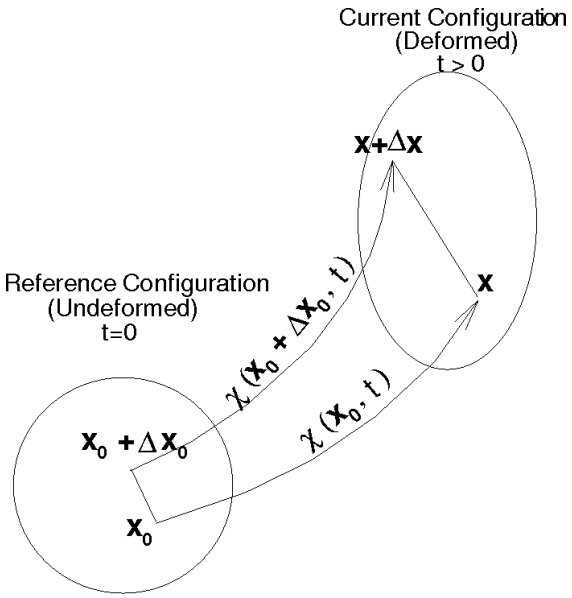

FIG. 2: Referential description of the kinematics of deformation.

any fluid motion has infinitely many different referential descriptions which are equally valid [3], it is convenient to choose the referential configuration corresponding to the fluid placement at the onset of the deformation (see Fig. 2). According to Truesdell [3], $\Omega(\mathbf{x}_0, t)$ and its derivatives with respect to $\mathbf{x}_0$ are supposed to be smooth functions of t and $\mathbf{x}_0$. Hence, if $\mathbf{x} = \boldsymbol{\chi}(\mathbf{x}_0, t)$ represents the fluid motion, Ω is expressed in terms of the geometrical position $\mathbf{x}$, through the inverse of $\boldsymbol{\chi}$, $\mathbf{x}_0 = \boldsymbol{\chi}^{-1}(\mathbf{x}, t)$

$$\Omega(\mathbf{x}, t) = \Omega(\boldsymbol{\chi}^{-1}(\mathbf{x}, t), t) \tag{12}$$

and its derivative with respect to $\mathbf{x}$ is

$$\frac{\partial \Omega}{\partial \mathbf{x}} = \frac{\partial \Omega}{\partial \mathbf{x}_0} \frac{\partial \mathbf{x}_0}{\partial \mathbf{x}} \tag{13}$$

The bifurcations of Eq. (1) make $\boldsymbol{\chi}$ a singular transformation, thus, in proximity of a bifurcation, $\partial\Omega/\partial\mathbf{x}$ varies much more quickly than $\partial\Omega/\partial\mathbf{x}_0$ because of the local stretching $\partial\mathbf{x}/\partial\mathbf{x}_0$, which is here calculated with the Lyapunov theory, as

$$\frac{\partial \mathbf{x}}{\partial \mathbf{x}_0} \approx \mathrm{e}^{\Lambda t} \tag{14}$$

where $\Lambda = \max(\Lambda_1, \Lambda_2, \Lambda_3)$ is the maximal Lyapunov exponent and Λ_i, $(i = 1, 2, 3)$ are the Lyapunov exponents. Due to the incompressibility, $\Lambda_1 + \Lambda_2 + \Lambda_3 = 0$, thus, $\Lambda > 0$.

The velocity fluctuation of the particle $\mathbf{x}_0$ -or Lagrangian fluctuation- is calculated using the momentum equations, where stress tensor and velocity field are mapped with respect to the referential coordinates at the beginning of the deformation

$$\left(\frac{\partial u_k}{\partial t}\right)_{\mathbf{x}_0} = \frac{1}{\rho} \frac{\partial T_{kh}}{\partial x_{j0}}(\mathbf{x}_0, t) \frac{\partial x_{j0}}{\partial x_h}(\mathbf{x}_0, t) \tag{15}$$

where $(\partial u_k/\partial t)_{\mathbf{x}_0}$ is the acceleration of the particle $\mathbf{x}_0$, whereas T_{kh} represents the stress tensor

$$T_{hk} = -p\delta_{hk} + \nu\rho \left(\frac{\partial u_h}{\partial x_k} + \frac{\partial u_k}{\partial x_h}\right) \tag{16}$$

Note that, Eq. (15) is more general than the classical Navier-Stokes equations, since it can be applied to fluid particles which exhibit non-smooth displacements and irregular boundaries [3], as in the present case. Since $\partial\mathbf{x}/\partial\mathbf{x}_0$ is much more rapid than $\partial T_{kh}/\partial x_{j0}$, this fluctuation is calculated integrating Eq. (15) from $t = 0$ to ∞, considering $\partial T_{kh}/\partial x_{j0}$ constant with respect to $\partial\mathbf{x}/\partial\mathbf{x}_0$, i.e.

$$u_k(\mathbf{x}_0) \approx \frac{1}{\Lambda}\left(-\frac{1}{\rho}\frac{\partial p}{\partial x_k} + \nu\nabla^2 u_k\right) = \frac{1}{\Lambda}\left(\frac{\partial u_k}{\partial t}\right)_{\mathbf{x}_0} \tag{17}$$

The velocity fluctuation in a fixed point of space $\mathbf{x}$ -or Eulerian fluctuation- is calculated taking into account the expression of the Eulerian time derivative of u_k, which is [3]

$$\left(\frac{\partial u_k}{\partial t}\right)_{\mathbf{x}} = \left(\frac{\partial u_k}{\partial t}\right)_{\mathbf{x}_0} - \frac{\partial u_k}{\partial x_{h0}}(\mathbf{x}_0, t)\frac{\partial x_{h0}}{\partial x_j}u_j \tag{18}$$

Therefore, this velocity fluctuation is

$$u_k(\mathbf{x}) \approx \frac{1}{\Lambda}\left(\frac{\partial u_k}{\partial t}\right)_{\mathbf{x}} \tag{19}$$

These velocity fluctuations, which stem from the bifurcations of the velocity field, do not modify the average values of the momentum and of the kinetic energy of fluid.

IV. LYAPUNOV ANALYSIS OF THE RELATIVE KINEMATICS

In order to investigate the mechanism of the energy cascade, the properties of the relative kinematic equations are here studied with the Lyapunov analysis. These equations are

$$\frac{d\mathbf{x}}{dt} = \mathbf{u}(\mathbf{x}, t), \quad \frac{d\mathbf{x}'}{dt} = \mathbf{u}(\mathbf{x}', t) \tag{20}$$

where $\mathbf{u}(\mathbf{x}, t) = (u_1, u_2, u_3)$, $\mathbf{u}(\mathbf{x}', t) \equiv \mathbf{u}' = (u_1', u_2', u_3')$, whereas u_i and u_i' are the velocity components expressed in the reference frame $\Re$. Since the bifurcations do not modify the total momentum and kinetic energy, the solutions of Eq. (20) preserve these quantities. With reference to Fig. 3, these solutions correspond to the paths, $\mathbf{x}(t)$ and $\mathbf{x}'(t)$, located into a material volume $\Sigma(t)$ which changes its geometry according to the fluid motion [18], whereas its volume remains unaltered. This is a toroidal volume, where S_p and R are, respectively, the poloidal surface and the toroidal dimension of Σ, whereas $\mathbf{X}$ and $\mathbf{X}'$ are the intersections of $\mathbf{x}(t)$ and $\mathbf{x}'(t)$ with S_p, where $r = |\mathbf{X}' - \mathbf{X}|$ is the poloidal dimension, thus $S_p \approx r^2$. The velocity difference components $\Delta u_n \equiv u_n' - u_n$ and $\Delta u_r \equiv u_r' - u_r$ lay on S_p and are normal and parallel to r, respectively, whereas u_b is the average velocity component along the direction normal to S_p. The equations describing the evolution of these quantities preserve the volume and the momentum of Σ. These can be written as

$$\frac{d}{dt}\left(S_p R\right) = 0 \tag{21}$$

$$\frac{d}{dt}\left(\Delta u_n^2 S_p\right) = 0 \tag{22}$$

$$\frac{d}{dt}\left(u_b R\right) = 0$$

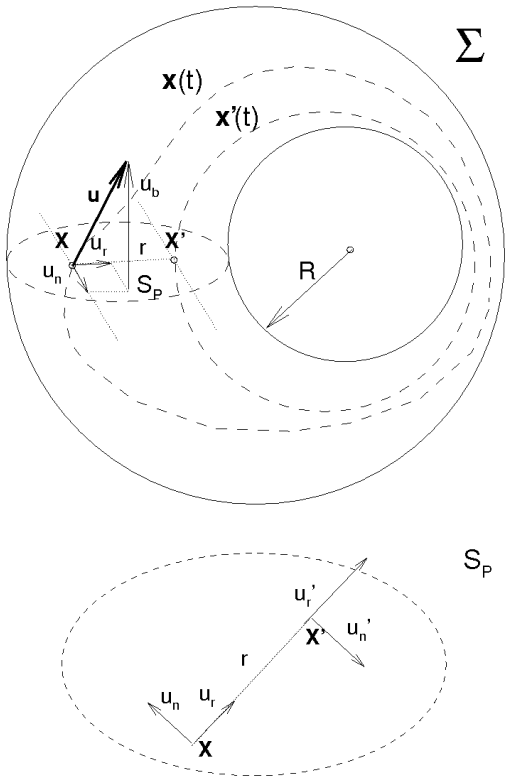

FIG. 3: Scheme of the relative kinematics of two fluid particles

Equations (21) and (22) represent, respectively, the continuity equation, and the momentum equations according to the third Helmholtz theorem on the vorticity [3, 18].

The Lyapunov analysis, applied to Eqs. (21) and (22), states that $R \approx R_0\ \mathrm{e}^{\lambda t}$, hence, Eqs. (21) and (22) become

$$\frac{d\Delta u_r^2}{dt} = -\lambda \Delta u_r^2$$

$$\frac{d\Delta u_n^2}{dt} = \lambda \Delta u_n^2 \tag{23}$$

$$\frac{du_b}{dt} = -\lambda u_b$$

where $\lambda(r) > 0$ is the maximal finite scale Lyapunov exponents associated to Eqs. (20), with $\lambda(0) = \Lambda$. As the result, $u_b \to 0$ and $\Delta\mathbf{u} \approx \Delta u_n \propto \mathrm{e}^{\lambda/2t}$.

Now, it is worth to remark that the following quantity

$$\Upsilon \equiv \frac{d}{dt}\left(\mathbf{u}\cdot\mathbf{u}'\right) \tag{24}$$

expresses the transfer of the kinetic energy between the points $\mathbf{x}$ and $\mathbf{x}'$. Its average $\langle \Upsilon \rangle$ is calculated on the ensemble of the diverse pairs of trajectories which pass through $\mathbf{X}$ and $\mathbf{X}'$ and which are contained into the various toroidal volumes. This average is obtained from Eqs. (23), taking into account the homogeneity, the isotropy and the time independence upon the time of the average kinetic energy ($d\langle \mathbf{u} \cdot \mathbf{u} \rangle / dt = 0$).

$$\langle \Upsilon \rangle = \langle \frac{d}{dt} \sum_{i=r,n,b} u_i u_i' \rangle = \lambda \; u^2 \; (g - f) \tag{25}$$

f and g are longitudinal and lateral velocity correlation functions, that, because of the incompressibility, are related each other through Eq. (60) (see Appendix). Thus, $\langle \Upsilon \rangle$ is

$$\langle \Upsilon \rangle = \frac{1}{2} u^2 \frac{\partial f}{\partial r} \; \lambda(r) r \tag{26}$$

If Υ were an ergodic function, its average on the statistical ensemble should coincide with the average over time which in turn is equal to zero since Υ is the time derivative of $\mathbf{u} \cdot \mathbf{u}'$. As the consequence, there would not be any transfer of energy between the parts of fluid. Therefore, the fluid incompressibility is a sufficient condition to state that Υ is a non ergodic function, whose statistical average is determined as soon as λ is known. To calculate λ, it is convenient to express the velocity difference $\Delta \mathbf{u} = \mathbf{u}(\mathbf{x}', t) - \mathbf{u}(\mathbf{x}, t)$ in the Lyapunov basis E associated to Eqs. (20), which is made by orthonormal vectors arising from Eqs. (20) [19, 20]. The velocity difference expressed in E, $\Delta \mathbf{v} \equiv (v_1' - v_1, \; v_2' - v_2, \; v_3' - v_3)$, satisfies the following equations, which hold for $t \to \infty$

$$v_i' - v_i = \lambda_i \; \hat{r}_i, \quad i = 1, 2, 3 \tag{27}$$

where $\hat{r}_i$, v_i and v_i' are, respectively, the components of $\hat{\mathbf{r}} \equiv \mathbf{x}' - \mathbf{x}$, $\mathbf{u}(\mathbf{x}, t)$ and $\mathbf{u}(\mathbf{x}', t)$ written in E. Then, Δu_r and r can be expressed in terms of $\Delta \mathbf{v}$ and $\hat{\mathbf{r}}$ as

$$r \approx \boldsymbol{\xi} \cdot \mathbf{Q} \hat{\mathbf{r}}, \quad \Delta u_r \approx \boldsymbol{\xi} \cdot \mathbf{Q} \Delta \mathbf{v} \tag{28}$$

Into Eqs. (28), $\mathbf{Q}$ is the fluctuating rotation matrix transformation from E to $\Re$, and $\boldsymbol{\xi} = (\mathbf{X}' - \mathbf{X}) / |\mathbf{X}' - \mathbf{X}|$. The standard deviation of Δu_r is calculated from Eqs. (28), taking into account the isotropy and that $\Delta \mathbf{v} \approx \lambda \hat{\mathbf{r}}$

$$\left\langle \Delta u_r^2(r) \right\rangle = \lambda^2 r^2 \tag{29}$$

This standard deviation can be also expressed through the longitudinal correlation function f

$$\langle \Delta u_r^2(r) \rangle = 2u^2(1 - f(r)) \tag{30}$$

being u the standard deviation of the longitudinal velocity. The maximal Lyapunov exponent is calculated in function of f, from Eqs. (29) and (30)

$$\lambda(r) = \frac{u}{r}\sqrt{2\,(1 - f(r))} \tag{31}$$

Hence, substituting Eq. (31) into Eq. (26), one obtains the expression of $\langle \Upsilon \rangle$ in terms of the longitudinal correlation function

$$\langle \Upsilon \rangle = u^3 \sqrt{\frac{1-f}{2}}\ \frac{\partial f}{\partial r} \tag{32}$$

where, thanks to the isotropy, $\langle \Upsilon \rangle$ is a function of r alone.

Equation (32) reflects the well known property of the inertia forces of transferring the kinetic energy [7] between the several regions of the fluid domain.

V. CLOSURE OF THE VON KÁRMÁN-HOWARTH EQUATION

The closure of the von Kármán-Howarth equation is now carried out using the previous Lyapunov analysis.

The function $K(r)$ is defined through the following relation (see also Eq. (62) in the Appendix)

$$\frac{\partial}{\partial r_k} \langle u_i u_i' (u_k - u_k') \rangle = \frac{\partial K(r)}{\partial r} r + 3K(r) \tag{33}$$

The repeated indexes into Eq. (33), i and k, indicate the summations with respect to the same indexes. In order to obtain the expression of $K(r)$, it is worth to remark the following identity

$$u_i u_i' (u_k - u_k') = \Upsilon\ r_k - \frac{d}{dt}(u_i u_i' r_k) \tag{34}$$

The average of Eq. (34) is calculated on the ensemble of the trajectories passing through $\mathbf{X}$ and $\mathbf{X}'$. It is supposed that the ergodic hypothesis holds for the last term at the right hand-side of Eq. (34), thus this latter can be calculated through the average over time. Since

this term is the time derivative of $u_i u_i' r_k$, this gives null contribution. Hence, accounting for the isotropy, one obtains

$$\frac{\partial}{\partial r_k}\langle u_i u_i'(u_k - u_k')\rangle = \frac{\partial\langle\Upsilon\rangle}{\partial r} r + 3\langle\Upsilon\rangle \tag{35}$$

Comparing Eqs. (33) and (35), and taking into account that $K(0) = 0$ [7], $K(r) \equiv \langle\Upsilon\rangle$, i.e.

$$K(r) = u^3\sqrt{\frac{1-f}{2}}\,\frac{\partial f}{\partial r} \tag{36}$$

Equation (36) represents the proposed closure of the von Kármán-Howarth equation, and expresses the transfer of kinetic energy between the diverse fluid regions. This is a kinematic mechanism, caused by the bifurcations cascades of Eq. (20), which preserves total momentum and kinetic energy. The analytical structure of Eq.(36) states that this mechanism consists of a flow of the kinetic energy from large to small scales which only redistributes the kinetic energy between wavelengths.

The skewness of Δu_r is determined once $K(r)$ is known [7]. This is

$$H_3(r) = \frac{\langle\Delta u_r^3\rangle}{\langle\Delta u_r^2\rangle^{3/2}} = \frac{6k(r)}{(2(1-f(r)))^{3/2}} \tag{37}$$

The longitudinal triple correlation $k(r)$ is calculated by Eq. (63) (see Appendix). Since f and k are, respectively, even and odd functions of r with $f(0) = 1$, $k(0) = k'(0) = k''(0) = 0$, $H_3(0)$ is given by

$$H_3(0) = \lim_{r\to 0} H_3(r) = \frac{k'''(0)}{(-f''(0))^{3/2}} \tag{38}$$

where the apex denote the derivative with respect to r. To obtain $H_3(0)$, observe that, near the origin, K behaves as

$$K = u^3\sqrt{-f''(0)}f''(0)\frac{r^2}{2} + O(r^4) \tag{39}$$

then, substituting Eq. (39) into Eq. (63) (see Appendix) and accounting for Eq. (38), one obtains

$$H_3(0) = -\frac{3}{7} = -0.42857... \tag{40}$$

This value of $H_3(0)$ is a constant of the present theory, which does not depend on the Reynolds number. This is in agreement with the several sources of data existing in the literature such as [7, 21, 22, 23] (and Refs. therein) and the knowledge of it gives the entity of the mechanism of energy cascade.

VI. STATISTICAL ANALYSIS OF VELOCITY DIFFERENCE

Although the previous analysis leads to the closure of the von Kármán-Howarth equation, it does not give any information about the statistics of velocity difference $\Delta\mathbf{u}(\mathbf{r}) \equiv \mathbf{u}(\mathbf{x}+\mathbf{r}) - \mathbf{u}(\mathbf{x})$.

In this section, the statistical properties of $\Delta\mathbf{u}(\mathbf{r})$, are investigated through the Fourier analysis of the velocity fluctuation given by Eq. (19). This fluctuation is

$$\mathbf{u} = \sum_{\boldsymbol{\kappa}} \mathbf{U}(\boldsymbol{\kappa}) \mathrm{e}^{i\boldsymbol{\kappa}\cdot\mathbf{x}} \approx \frac{1}{\Lambda} \sum_{\boldsymbol{\kappa}} \frac{\partial \mathbf{U}}{\partial t}(\boldsymbol{\kappa}) \mathrm{e}^{i\boldsymbol{\kappa}\cdot\mathbf{x}} \tag{41}$$

where $\mathbf{U}(\boldsymbol{\kappa}) \equiv (U_1(\boldsymbol{\kappa}), U_2(\boldsymbol{\kappa}), U_3(\boldsymbol{\kappa}))$ are the components of velocity spectrum, which satisfy [7]

$$\begin{aligned} &\frac{\partial U_p(\boldsymbol{\kappa})}{\partial t} = -\nu k^2 U_p(\boldsymbol{\kappa}) + \\ &i \sum_{\mathbf{j}} \left(\frac{\kappa_p \kappa_q \kappa_r}{\kappa^2} U_q(\mathbf{j}) U_r(\boldsymbol{\kappa}-\mathbf{j}) - \kappa_q U_q(\mathbf{j}) U_p(\boldsymbol{\kappa}-\mathbf{j}) \right) \end{aligned} \tag{42}$$

All the components $\mathbf{U}(\boldsymbol{\kappa}) \approx \partial\mathbf{U}(\boldsymbol{\kappa})/\partial t/\Lambda$ are random variables distributed according to certain distribution functions, which are statistically orthogonal each other [7].

Thanks to the local isotropy, $\mathbf{u}$ is sum of several dependent random variables which are identically distributed [7], therefore $\mathbf{u}$ tends to a gaussian variable [24], and $\mathbf{U}(\boldsymbol{\kappa})$ satisfies the Lindeberg condition, a very general necessary and sufficient condition for satisfying the central limit theorem [24]. This condition does not apply to the Fourier coefficients of $\Delta\mathbf{u}$. In fact, since $\Delta\mathbf{u}$ is the difference between two dependent gaussian variables, its PDF could be a non gaussian distribution function. In $\mathbf{x} = 0$, the velocity difference $\Delta\mathbf{u}(\mathbf{r}) \equiv (\Delta u_1, \Delta u_2, \Delta u_3)$ is given by

$$\Delta u_p \approx \frac{1}{\Lambda} \sum_{\boldsymbol{\kappa}} \frac{\partial U_p(\boldsymbol{\kappa})}{\partial t} (\mathrm{e}^{i\boldsymbol{\kappa}\cdot\mathbf{r}} - 1) \equiv L + B + P + N \tag{43}$$

This fluctuation consists of the contributions appearing into Eq. (42): in particular, L represents the sum of all linear terms due to the viscosity and B is the sum of all bilinear terms arising from inertia and pressure forces. P and N are, respectively, the sums of definite positive and negative square terms, which derive from inertia and pressure forces. The quantity $L + B$ tends to a gaussian random variable being the sum of statistically

orthogonal terms [24, 25], while P and N do not, as they are linear combinations of squares [25]. Their general expressions are [25]

$$\begin{aligned} P &= P_0 + \eta_1 + \eta_2^2 \\ N &= N_0 + \zeta_1 + \zeta_2^2 \end{aligned} \tag{44}$$

where P_0 and N_0 are constants, and η_1, η_2, ζ_1 and ζ_2 are four different centered random gaussian variables. Therefore, the fluctuation Δu_p with zero average reads as

$$\Delta u_p = \psi_1(\mathbf{r})\xi + \psi_2(\mathbf{r})\left(\chi(\eta^2 - 1) - (\zeta^2 - 1)\right) \tag{45}$$

where ξ, η and ζ are independent centered random variables which have gaussian distribution functions with standard deviation equal to the unity. The parameter χ is a function of Reynolds number, whereas ψ_1 and ψ_2 are functions of space coordinates, which also depend on the Reynolds number.

At the Kolmogorov scale the order of magnitude of the velocity fluctuations is ${u_K}^2\tau/\ell$, with $\tau = 1/\Lambda$, and ψ_2 is negligible because is due to the inertia forces: this immediately identifies $\psi_1 \approx {u_K}^2\tau/\ell$.

On the contrary, at the Taylor scale, ψ_1 is negligible and the order of magnitude of the velocity fluctuations is $u^2\tau/\lambda_T$, therefore $\psi_2 \approx u^2\tau/\lambda_T$ and the ratio ψ_2/ψ_1 is a function of R_λ

$$\psi(\mathbf{r}, R_\lambda) = \frac{\psi_2(\mathbf{r})}{\psi_1(\mathbf{r})} \approx \frac{u^2\ell}{{u_K}^2\lambda_T} = \sqrt{\frac{R_\lambda}{15\sqrt{15}}}\,\hat{\psi}(\mathbf{r}, R_\lambda) \tag{46}$$

where $\hat{\psi}(\mathbf{r}, R_\lambda) = O(1)$, is a function which has to be determined. Hence, the longitudinal velocity difference Δu_r, is written as

$$\frac{\Delta u_r}{\sqrt{\langle {\Delta u_r}^2 \rangle}} = \frac{\xi + \psi\left(\chi(\eta^2 - 1) - (\zeta^2 - 1)\right)}{\sqrt{1 + 2\psi^2\left(1 + \chi^2\right)}} \tag{47}$$

The quadratic term at the right hand side of Eq. (47) represents the velocity fluctuations at the bigger scales, and there is no physical reason for which this must be bounded between same limits. Consequentely, χ must be a definite positive function of R_λ.

Equation (47) gives the mathematical structure of Δu_r, whose dimensionless statistical

moments are easily calculated considering that ξ, η and ζ are independent gaussian variables

$$H_n \equiv \frac{\langle \Delta u_r^n \rangle}{\langle \Delta u_r^2 \rangle^{n/2}} = \frac{1}{(1+2\psi^2\,(1+\chi^2))^{n/2}}$$
$$\sum_{k=0}^{n} \binom{n}{k} \psi^k \langle \xi^{n-k} \rangle \langle (\chi(\eta^2-1)-(\zeta^2-1))^k \rangle \tag{48}$$

where

$$\langle (\chi(\eta^2-1)-(\zeta^2-1))^k \rangle =$$
$$\sum_{i=0}^{k} \binom{k}{i} (-\chi)^i \langle (\zeta^2-1)^i \rangle \langle (\eta^2-1)^{k-i} \rangle \tag{49}$$
$$\langle (\eta^2-1)^i \rangle = \sum_{l=0}^{i} \binom{i}{l} (-1)^l \langle \eta^{2(i-l)} \rangle$$

In particular, the third moment or skewness, H_3, which is responsible for the energy cascade, is

$$H_3 = \frac{8\psi^3\,(\chi^3-1)}{(1+2\psi^2\,(1+\chi^2))^{3/2}} \tag{50}$$

For $\chi \neq 1$, the skewness and all the odd order moments are different from zero, and for $n > 3$, all the absolute moments are rising functions of R_λ, thus Δu_r exhibits an intermittency whose entity increases with the Reynolds number. If H_3 and χ were both known, the other statistical moments can be consequentely calculated with Eq. (48). The function $\psi(r, R_\lambda)$ is determined for Δu_r from Eqs. (50) and (37). For r=0, one obtains the relationship

$$\frac{8{\psi_0}^3\,(1-\chi^3)}{\left(1+2{\psi_0}^2\,(1+\chi^2)\right)^{3/2}} = \frac{3}{7} \tag{51}$$

$\psi_0 = \psi(0, R_\lambda)$ =O(1), is given by Eq. (46), where, its exact value has to be calculated, whereas χ is a positive function of R_λ which must also be determined. To determine such quantities, note that Eq.(51) is an algebraic relationship which gives χ in terms of R_λ, as shown in Fig. 4. In any case, χ exhibits the limit $\chi \simeq 0.86592$ for $R_\lambda \to \infty$, whereas R_λ admits the minimim $(R_\lambda)_{min}$ which depends on $\hat{\psi}_0$. Below such minimum, Eq. (51) does not admit solutions with $\chi > 0$. Then, according to the analysis of section II A, $\hat{\psi}_0$ is chosen

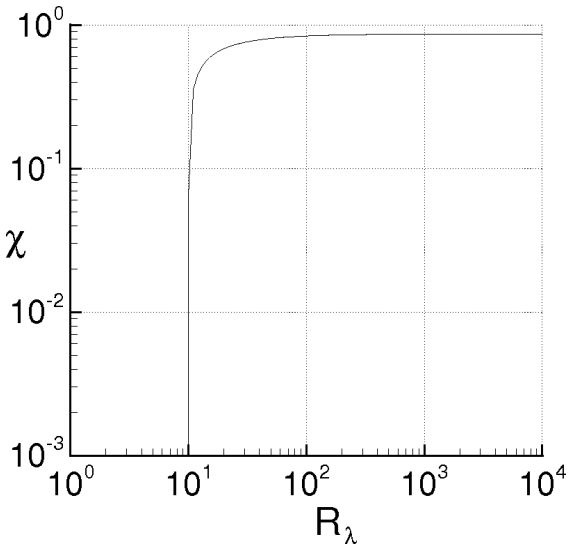

FIG. 4: Parameter χ plotted as the function of R_λ.

in such a way that $(R_\lambda)_{min} = 10.12$ as shown in Fig. 4, resulting $\hat{\psi}_0 \simeq 1.075$. Now, all the moments of Δu_r can be calculated by Eqs. (48) and (49) in terms of R_λ.

The PDF of Δu_r is expressed through the Frobenious-Perron equation

$$F(\Delta u'_r) = \int_\xi \int_\eta \int_\zeta p(\xi)p(\eta)p(\zeta)\ \delta\left(\Delta u_r - \Delta u'_r\right) d\xi d\eta d\zeta \tag{52}$$

where Δu_r is calculated with Eq. (47), δ is the Dirac delta and p is a gaussian PDF whose average value and standard deviation are equal to 0 and 1, respectively.

For non-isotropic turbulence or in more complex cases with boundary conditions, the velocity spectrum could not satisfy the Lindeberg condition, thus the velocity will be not distrubuted following a Gaussian PDF, and Eq. (45) changes its analytical form and can incorporate more intermittant terms [24] which give the deviation with respect to the isotropic turbulence. Hence, the absolute statistical moments of Δu_r will be greater than those calculated with Eq. (47), indicating that, in a more complex situation than the isotropic turbulence, the intermittancy of Δu_r can be significantly stronger.

VII. RESULTS AND DISCUSSION

The results calculated with the proposed theory are now presented.

As the first result, the evolution in time of the correlation function is calculated with the proposed closure of the von Kármán-Howarth equation (Eq. (36)), where the boundary

conditions are given by Eq. (65). The turbulent kinetic energy and the spectrums $E(\kappa)$ and $T(\kappa)$ are calculated with Eq. (66) and Eqs. (67), respectively. The calculation is carried out for the initial Reynolds number of $Re = u(0)L_r/\nu = 2000$, where L_r and $u(0)$ are, respectively, the characteristic dimension of the problem and the initial velocity standard deviation. The initial condition is a gaussian correlation function with $\lambda_T/L_r = 1/(2\sqrt{2})$. The dimensionless time of the problem is defined as $\bar{t} = t\ u(0)/L_r$.

Equation (61) was numerically solved adopting the Crank-Nicholson integrator scheme with variable time step, where the discretization of the space domain is made by $N-1$ intervals of the same amplitude Δr. This corresponds to a discretization of the Fourier space made by $N-1$ subsets in the interval $[0, \kappa_M]$, where $\kappa_M = \pi/(2\Delta r)$. For the adopted initial Reynolds number, the choice $N = 1500$, gives an adequate discretization, which provides $\Delta r < \ell$, for the whole simulation. During the simulation, $T(\kappa)$ must identically satisfy Eq.(68) (see Appendix) which states that $T(\kappa)$ does not modify the kinetic energy. To verify Eq.(68), the integral of $T(\kappa)$ is calculated with the trapezes rule from 0 until to κ_M, at each time step, therefore, the simulation will be considered to be accurate as long as

$$\int_0^{\kappa_M} T(\kappa)d\kappa \simeq \int_0^{\infty} T(\kappa)d\kappa = 0 \tag{53}$$

namely, when the energy is distributed for $\kappa < \kappa_M$. As the simulation advances, according to Eq. (36), the energy cascade determines variations of $E(\kappa)$ and $T(\kappa)$ at the higher wave-numbers, then Eq. (53) will hold until to a certain time. For this reason, the simulation is stopped as soon as the following condition is achieved [26]

$$|\int_0^{\kappa_M} T(\kappa)d\kappa| > \frac{1}{N^2}\int_0^{\kappa_M} |T(\kappa)|d\kappa \tag{54}$$

At the end of several simulations, we have $\Delta r \approx 0.8\ \ell$, and, in this situation, the energy spectrum is here considered to be fully developed.

The diagrams of Fig. 5 show the correlation functions $f(r)$ and $k(r)$ vs. the dimensionless distance r/λ_T, at different times of simulation. The kinetic energy and Taylor scale diminish according to Eqs. (36) and (66), thus $f(r)$ and $k(r)$ change in such a way that the length scales associated to their variations diminish as the time increases, whereas the maximum of $|k|$ decreases. At the final instants of the simulation, one obtains that $f - 1 = \mathrm{O}(\ r^{2/3})$ for $r/\lambda_T = \mathrm{O}(1)$, whereas the maximum of $|k|$ is about 0.05. These results are in very good agreement with the numerous data of the literature [7] which concern the evolution of

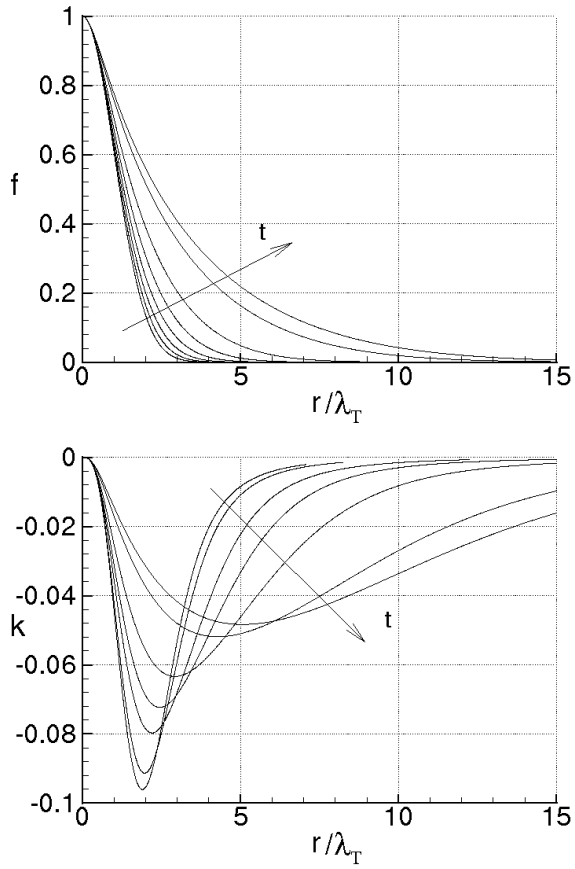

FIG. 5: Correlation functions, f and k versus the separation distance at the times of simulation $\bar{t}$ = 0, 0.1, 0.2, 0.3, 0.4, 0.5, 0.6, 0.63.

correlation function and energy spectrum. Figure 6 shows the diagrams of $E(\kappa)$ and $T(\kappa)$ for the same times, where the dashed line in the plot of $E(\kappa)$, represents the $-5/3$ Kolmogorov law [5]. The spectrums $E(\kappa)$ and $T(\kappa)$ vary according to Eqs. (36) and (67), and, at the end of simulation, $E(\kappa)$ is about parallel to the dashed line in an opportune interval of the wave-numbers which defines the so called inertial range of Kolmogorov. This arises from the developed correlation function, which behaves like $f - 1 = \mathrm{O}\ (r^{2/3})$ for $r = O(\lambda_T)$.

Next, the Kolmogorov function $Q(r)$ and Kolmogorov constant C, are determined with the proposed theory, using the previous results of the simulation.

Following the Kolmogorov theory, the Kolmogorov function, which is defined as

$$Q(r) = -\frac{\langle \Delta {u_r}^3 \rangle}{r\varepsilon} \tag{55}$$

is constant with respect to r, and is equal to $4/5$ as long as $r/\lambda_T = O(1)$. As shown in Fig. 7, for $\bar{t} = 0$, the maximum of $Q(r)$ is much greater than $4/5$ and its variations with r/λ_T

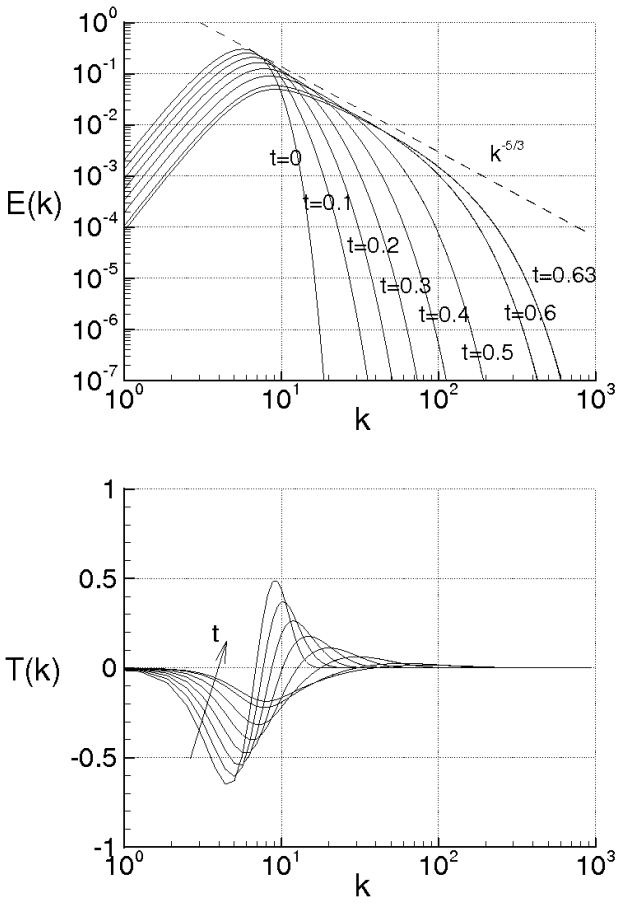

FIG. 6: Plot of $E(\kappa)$ and $T(\kappa)$ at the diverse times of simulation.

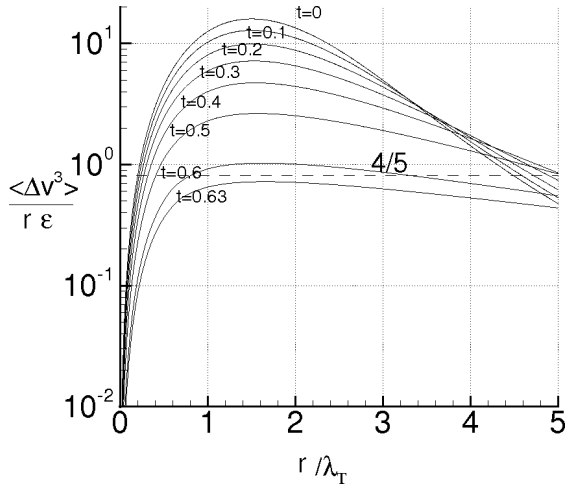

FIG. 7: The Kolmogorov function versus r/λ_T for different times of simulation. The dashed line indicates the value 4/5.

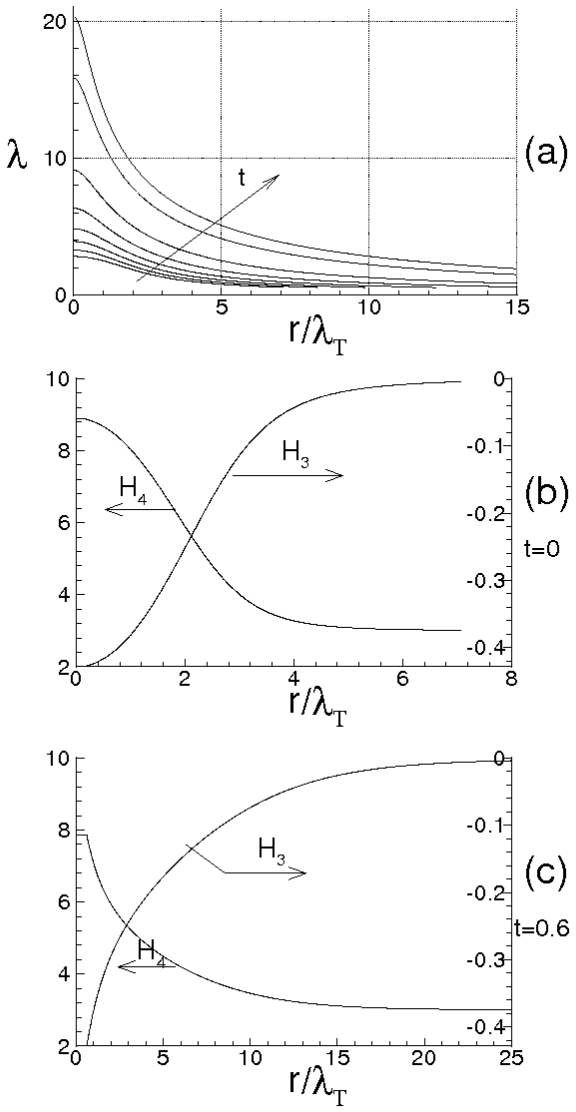

FIG. 8: (a) Maximum finite size Lyapunov exponent at the times of simulation $\bar{t} = 0$, 0.1, 0.2, 0.3, 0.4, 0.5, 0.6, 0.63; (b) and (c) skewness and Flatness versus r/λ_T at t = 0 and t = 0.6, respectively.

can not be neglected. This is due to the arbitrary choice of the initial correlation function. At the successive times, the variations of f determine that the maximum of $Q(r)$ and its variations decrease until to the final instants, where, with the exception of $r/\lambda_T \approx 0$, $Q(r)$ exhibits a qualitatively flat shape in a wide range of r/λ_T, with a maximum which is quite close to 0.8.

The Kolmogorov constant C is also calculated by definition

$$E(\kappa) = C\frac{\varepsilon^{2/3}}{\kappa^{5/3}} \tag{56}$$

This is here determined, as the value of C which makes the curve represented by Eq. (56)

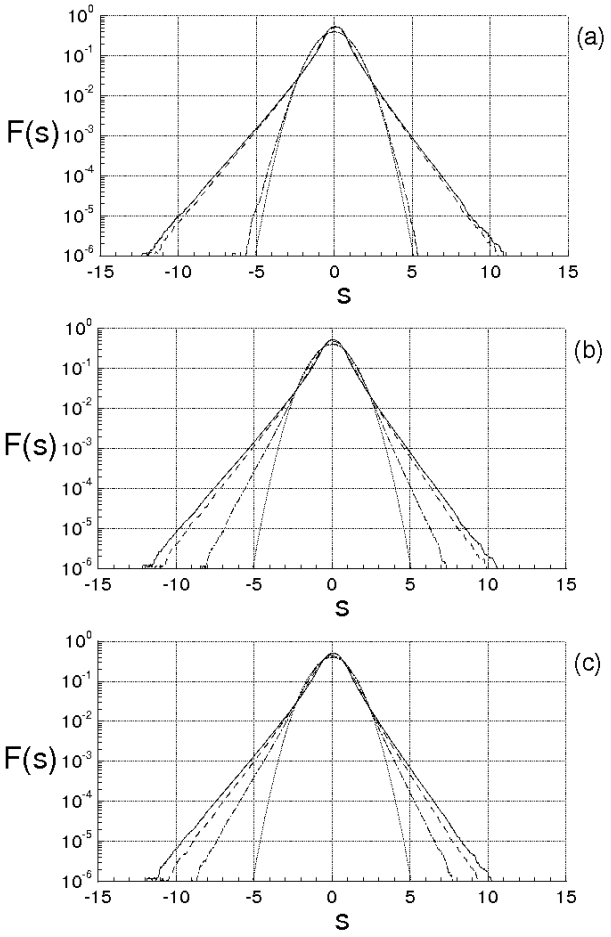

FIG. 9: PDF of the velocity difference fluctuations at the times $\bar{t}$ =0 (a), $\bar{t}$ = 0.5 (b) and $\bar{t}$ =0.6 (c). Continuous lines are for r =0, dashed lines are for r/λ_T =1, dot-dashed lines are for r/λ_T =5, dotted lines are for gaussian PDF.

to be tangent to the energy spectrum $E(\kappa)$ previously calculated. At end simulation, $C \simeq 1.932$, namely C and Q_{max} agree very well to the corresponding quantities known from the literature. For the same simulation, Fig. 8a shows the maximal finite scale Lyapunov exponent, calculated with Eq. (31), where λ varies according to f. For $t = 0$, the variations of λ are relatively small because of the adopted initial correlation function which is a gaussian, whereas as the time increases, the variations of f determine sizable increments of λ and of its slope in proximity of the origin. Then, for developed spectrum, since $f - 1 = \mathrm{O}(r^{2/3})$, the maximal finite scale Lyapunov exponent behaves like $\lambda \approx r^{-2/3}$. Thus, the diffusivity coefficient associated to the relative motion between two fluid particles, defined as $D(r) \propto \lambda r^2$, here satisfies the famous Richardson scaling law $D(r) \approx r^{4/3}$[4].

In the diagrams of Figs. 8b and 8c, skewness and flatness of Δu_r are shown in terms of r for $\bar{t} = 0$ and 0.6. The skewness, H_3 is first calculated with Eq. (37), then H_4 has been determined using Eq. (48). At $\bar{t} = 0$, $|H_3|$ starts from 3/7 at the origin with small slope, then decreases until to reach small values. H_4 also exhibits small derivatives near the origin, where $H_4 \gg 3$, thereafter it decreases more rapidly than $|H_3|$. At $\bar{t}$ =0.6, the diagram importantly changes and exhibits different shapes. The Taylor scale and the corresponding Reynolds number are both diminished, so that the variations of H_3 and H_4 are associated to smaller distances, whereas the flatness at the origin is slightly less than that at $t = 0$. Nevertheless, these variations correspond to higher r/λ_T than those for $t = 0$, and also in this case, H_4 reaches the value of 3 more rapidly than H_3 tends to zero.

The PDFs of Δu_r are calculated with Eqs. (52) and (47), and are shown in Fig. 9 in terms of the dimensionless abscissa

$$s = \frac{\Delta u_r}{\langle \Delta u_r^2 \rangle^{1/2}}$$

where, these distribution functions are normalized, in order that their standard deviations are equal to the unity. The figure represents the distribution functions of s for several r/λ_T, at $\bar{t} = 0$, 0.5 and 0.6, where the dotted curves represent the gaussian distribution functions. The calculation of $H_3(r)$ is first carried out with Eq. (37), then the function $\psi(r, R_\lambda)$ is identified through Eq. (50), and finally the PDF is obtained with Eq. (52). For $t = 0$ (see Fig. 9a) and according to the evolutions of H_3 and H_4, the PDFs calculated at $r/\lambda_T = 0$ and 1, are quite similar each other, whereas for $r/\lambda_T = 5$, the PDF is an almost gaussian function. Toward the end of the simulation, (see Fig. 9b and c), the two PDFs calculated at $r/\lambda_T = 0$ and 1, exhibit more sizable differences, whereas for $r/\lambda_T = 5$, the PDF differs very much from a gaussian PDF. This is in line with the plots of $H_3(r)$ and $H_4(r)$ of Fig. 8.

Next, the spatial structure of Δu_r, given by Eq. (47), is analyzed using the previous results of the simulation. According to the various works [27, 28, 29], Δu_r behaves quite similarly to a multifractal system, where Δu_r obeys to a law of the kind $\Delta u_r(r) \approx r^q$ where the exponent q is a fluctuating function of space. This implies that the statistical moments of $\Delta u_r(r)$ are expressed through different scaling exponents $\zeta(P)$ whose values depend on the moment order P, i.e.

$$\left\langle \Delta u_r^P(r) \right\rangle = A r^{\zeta(P)} \tag{57}$$

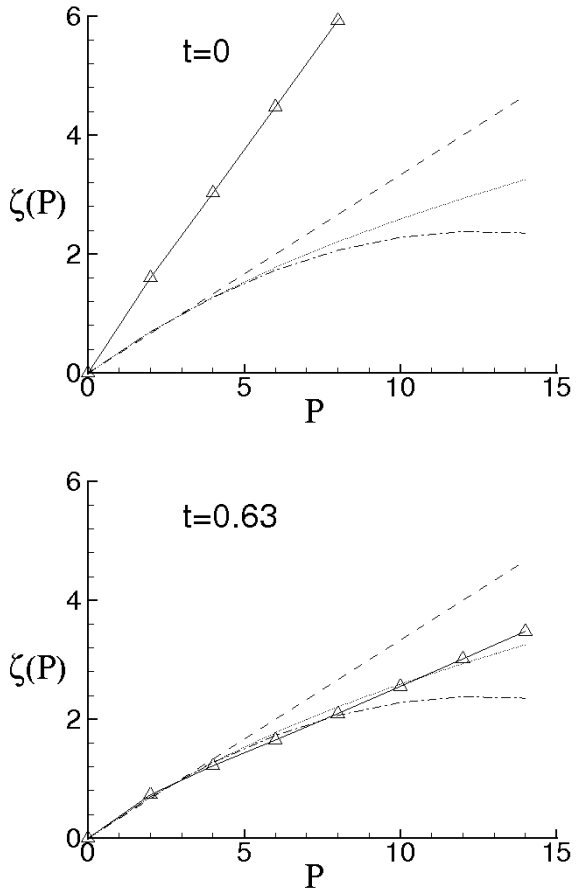

FIG. 10: Scaling exponents of longitudinal velocity difference versus the order moment at different times. Continuous lines with solid symbols are for the present data. Dashed lines are for Kolmogorov K41 data [5]. Dashdotted lines are for Kolmogorov K62 data [27]. Dotted lines are for She-Leveque data [28]

These scaling exponents are here identified through a best fitting procedure, in the interval $2\ell < r < \lambda_T$, where the statistical moments of $\Delta u_r(r)$ are calculated with Eqs. (48). Figure 10 shows the comparison between the scaling exponents here obtained (continuous lines with solid symbols) and those of the Kolmogorov theories K41 [5] (dashed lines) and K62 [27] (dashdotted lines), and those given by She-Leveque [28] (dotted curves). At $t = 0$, the slope of $\zeta(P)$ is about constant, whereas the values of $\zeta(P)$ are very different from those calculated by the various authors. This means that, for the chosen initial correlation function, $\Delta u_r(r)$ behaves like a simple fractal system, where $\zeta(P) \propto P$. Again, this result depends on the fact that, at the initial times, the energy spectrum is not developed. As the time increases, the correlation function changes causing variations in the statistical moments of $\Delta u_r(r)$. As

result, $\zeta(P)$ gradually diminish and exhibit a variable slope which depends on the moment order P, until to reach the situation of Fig. 10b, where the simulation is just ended. The correlation function and the dimensionless moments of $\Delta u_r(r)$ are changed, thus the plot of $\zeta(P)$ shows that near the origin, $\zeta(P) \simeq P/3$, whereas elsewhere the values of $\zeta(P)$ are in agreement with the She-Leveque results, confirming that $\Delta u_r(r)$ behaves like a multifractal system.

Other simulations with different initial correlation functions and Reynolds numbers have been performed, and all of them lead to analogous results, in the sense that, at the end of the simulations, the diverse quantities such as $Q(r)$, C and $\zeta(P)$ are quite similar to those just calculated. For what concerns the effect of the Reynolds number, its increment determines a wider Kolmogorov inertial range and a smaller dissipation energy rate in accordance to Eq. (66), whereas the shapes of the various energy spectrums remain qualitatively unaltered with respect to Fig. 6.

In order to study the evolution of the intermittancy vs. the Reynolds number, Table 1 gives the first ten statistical moments of $F(\partial u_r/\partial r)$. These are calculated with Eqs. (48) and (49), for $R_\lambda = 10.12$, 100 and 1000, and are shown in comparison with those of a gaussian distribution function. It is apparent that a constant nonzero skewness of the longitudinal velocity derivative, causes an intermittancy which rises with R_λ (see Eq. (47)).

Moment	$R_\lambda \approx 10$	$R_\lambda = 10^2$	$R_\lambda = 10^3$	Gaussian
Order	P. R.	P. R.	P. R.	Moment
3	-.428571	-.428571	-.428571	0
4	3.96973	7.69530	8.95525	3
5	-7.21043	-11.7922	-12.7656	0
6	42.4092	173.992	228.486	15
7	-170.850	-551.972	-667.237	0
8	1035.22	7968.33	11648.2	105
9	-6329.64	-41477.9	-56151.4	0
10	45632.5	617583.	997938.	945

TABLE I: Dimensionless statistical moments of $F(\partial u_r/\partial r)$ at different Taylor scale Reynolds numbers. P.R. as for "present results".

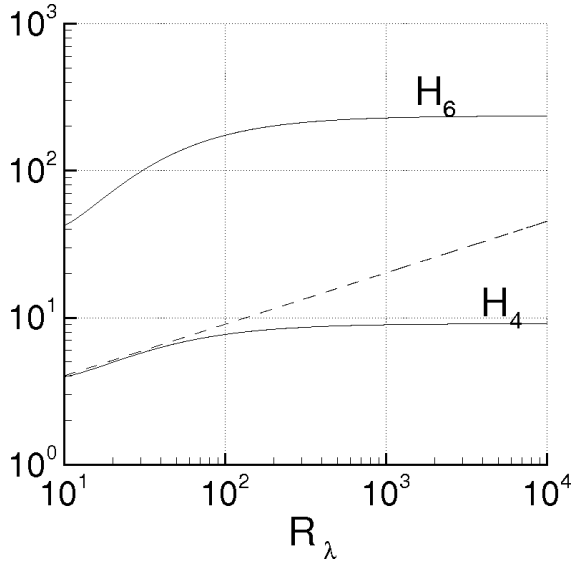

FIG. 11: Dimensionless moments $H_4(0)$ and $H_6(0)$ plotted vs. R_λ. Continuous lines are for the present results. The dashed line is the tangent to the curve of $H_4(0)$ in $R_\lambda \approx 10$.

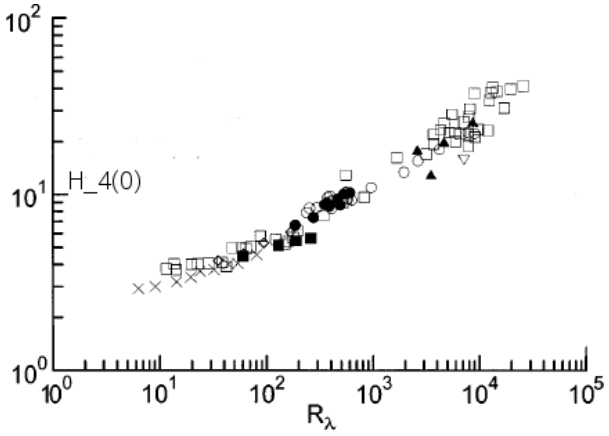

FIG. 12: Flatness $H_4(0)$ vs. R_λ. These data are from Ref.[21].

More specifically, Fig. 11 shows the variations of $H_4(0)$ and $H_6(0)$ (continuous lines) in terms of R_λ, calculated with Eqs. (48) and (49), with $H_3(0) = -3/7$. These moments are rising functions of R_λ for $10 \lesssim R_\lambda \lesssim 700$, whereas for higher R_λ these tend to the saturation and such behavior also happens for the other absolute moments. According to Eq. (48), in the interval $10 \lesssim R_\lambda \lesssim 70$, H_4 and H_6 result to be about proportional to $R_\lambda^{0.34}$ and $R_\lambda^{0.78}$, respectively, and the intermittancy increases with the Reynolds number until to $R_\lambda \approx 700$, where it ceases to rise so quickly. This behavior, represented by the continuous lines, depends on the fact that $\psi \approx \sqrt{R_\lambda}$, and results to be in very good agreement with the data

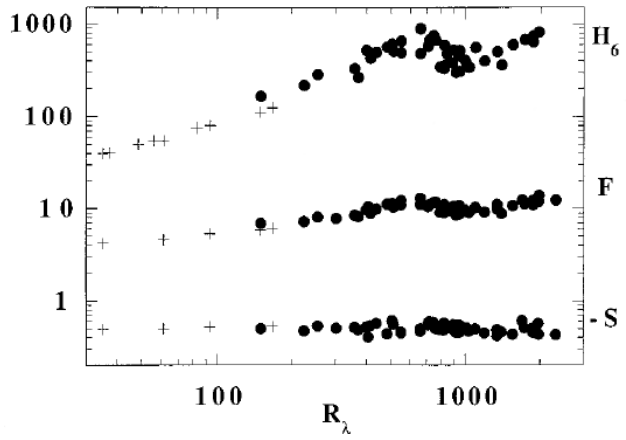

FIG. 13: Skewness $S = H_3(0)$, Flatness $F = H_4(0)$ and hyperflatness $H_6(0)$ vs. R_λ. These data are from Ref.[23].

of Pullin and Saffman [30], for $10 \lesssim R_\lambda \lesssim 100$. Figure 11 can be compared with the data collected by Sreenivasan and Antonia [21], which are here reported into Fig. 12. These latter are referred to several measurements and simulations obtained in different situations which can be very far from the isotropy and homogeneity conditions. Nevertheless a comparison between the present results and those of Ref. [21] is an opportunity to state if the two data exhibit elements in common. According to Ref. [21], the flatness monotonically rises with R_λ with a rising rate which agrees with Eq. (49) for $10 \lesssim R_\lambda \lesssim 60$ (dashed line, Fig. 11), whereas the skewness seems to exhibit minor variations. Thereafter, H_4 continues to rise with about the same rate, without the saturation observed in Fig. 11. The weaker intermittancy calculated with the present theory arise from the isotropy which makes the velocity fluctuation a gaussian random variable, while, as seen in sec. VI, without the isotropy condition, the flatness of velocity and of velocity difference can be much greater than that of the isotropic case.

Again, the obtained results are compared with the data of Tabeling *et al* [22, 23], where, in an experiment using low temperature helium gas between two counter-rotating cylinders (closed cell), the authors measure the PDF of $\partial u_r/\partial r$ and its moments. Also in this case the flow can be quite far from to the isotropy condition. In fact, these experiments pertain wall-bounded flows, where the walls could importantly influence the fluid velocity in proximity of the probe. The authors found that the higher moments than the third order, first increase with R_λ until to $R_\lambda \approx 700$, then exhibit a lightly non-monotonic evolution with respect to

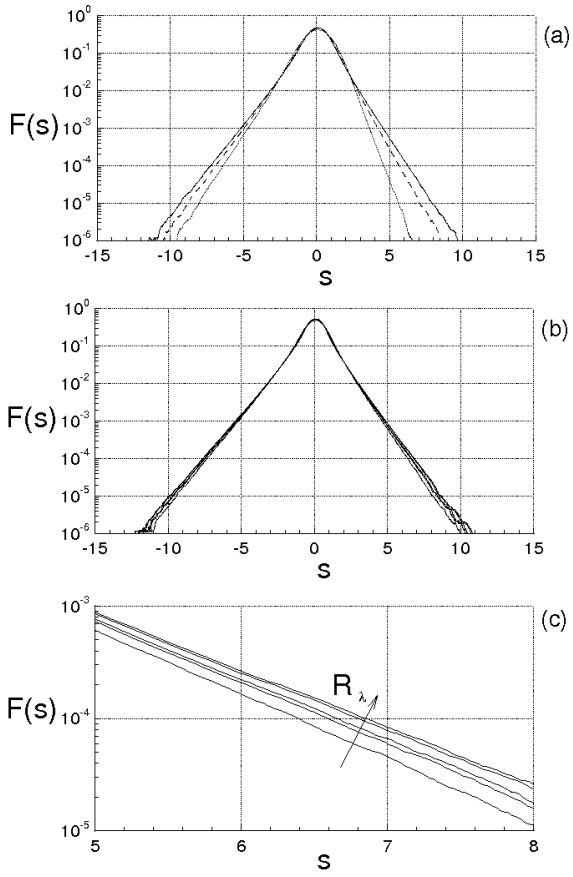

FIG. 14: Log linear plot of the PDF of $\partial u_r/\partial r$ for different R_λ. (a): dotted, dashdotted and continuous lines are for $R_\lambda = 15$, 30 and 60, respectively. (b) and (c) PDFs for $R_\lambda = 255$, 416, 514, 1035 and 1553. (c) represents an enlarged part of the diagram (b)

R_λ, and finally cease their variations denoting a transition behavior (See Fig. 13). As far as the skewness is concerned, the authors observe small percentage variations. Although the isotropy does not describe the non-monotonic evolution near $R_\lambda = 700$, the results obtained with Eq. (47) can be considered comparable with those of Refs. [22, 23], resulting also in this case, that the proposed theory gives a weaker intermittancy with respect to Refs. [22, 23].

The normalized PDFs of $\partial u_r/\partial r$ are calculated with Eqs. (52) and (47), and are shown in Fig. 14 in terms of the variable s, which is defined as

$$s = \frac{\partial u_r/\partial r}{\langle(\partial u_r/\partial r)^2\rangle^{1/2}}$$

Figure 14a shows the diagrams for $R_\lambda = 15$, 30 and 60, where the PDFs vary in such a way that $H_3(0) = -3/7$.

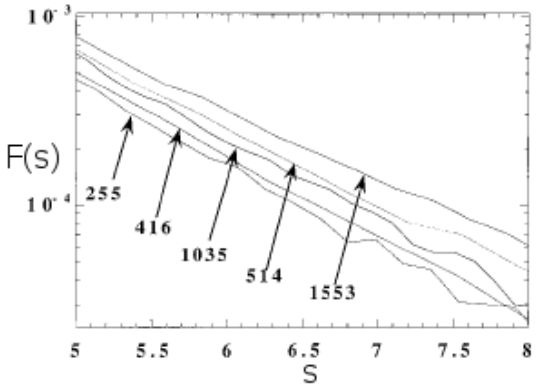

FIG. 15: PDF of $\partial u_r/\partial r$ for $R_\lambda = 255$, 416, 514, 1035 and 1553. These data are from Ref. [23]

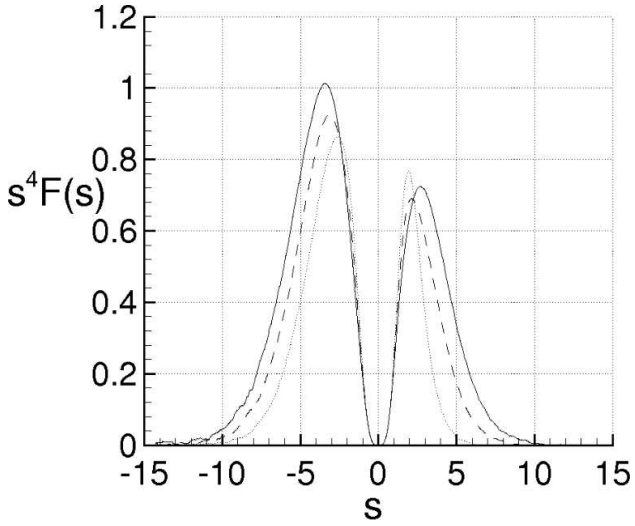

FIG. 16: Plot of the integrand $s^4F(s)$ for different R_λ. Dotted, dashdotted and continuous lines are for $R_\lambda = 15$, 30 and 60, respectively.

As well as in Ref. [23], Figs. 4b and 4c give the PDF for $R_\lambda = 255$, 416, 514, 1035 and 1553, where these last Reynolds numbers are calculated through the Kolmogorov function given in Ref. [23], with $H_3(0) = -3/7$. In particular, Fig. 14c represents the enlarged region of Fig. 14b, where the tails of PDF are shown for $5 < s < 8$. According to Eq. (47), the tails of the PDF rise in the interval $10 \lesssim R_\lambda \lesssim 700$, whereas at higher R_λ, smaller variations occur. Although the non-monotonic trend observed in Ref. [23], Fig. 14c shows that the values of the PDFs calculated with the proposed theory, for $5 < s < 8$, exhibit the same order of magnitude of those obtained by Tabeling *et al* [23] which are here shown in Fig. 15.

Asymmetry and intermittency of the distribution functions are also represented through

the integrand function of the 4^{th} order moment of PDF, which is $J_4(s) = s^4 F(s)$ This function is shown in terms of s, in Fig. 16, for $R_\lambda = 15$, 30 and 60.

VIII. CONCLUSIONS

The proposed theory is based on the Landau conjecture which states that the turbulence is caused by the bifurcations of the velocity field.

The obtained results confirm the capability of the proposed theory to describe quite well the general properties of the turbulence. These results are here summarized:

1. The analysis of the bifurcations gives the connection between number of bifurcations, length scales and Reynolds number at the onset of the turbulence and allows to determine the minimum Taylor-scale Reynolds number for isotropic turbulence. This last one is about 10, and, below this value, the isotropic turbulence is not allowed.

2. The momentum equations written using the referential description allow the velocity fluctuation to be expressed by means of the Lyapunov analysis of the kinematics of fluid deformation.

3. The Lyapunov analysis of the relative kinematics equations provides an explanation of the physical mechanism of the energy cascade in turbulence. The non-ergodicity of $d/dt(\mathbf{u} \cdot \mathbf{u}')$, due to the fluid incompressibility, make possible that the inertia forces transfer the kinetic energy between the length scales without changing the total kinetic energy. This implies that the skewness of the longitudinal velocity derivative is a constant of the present theory and that the energy cascade mechanism does not depend on the Reynolds number.

4. The Fourier analysis of the velocity difference provides the statistics of Δu_r. This is a non-Gaussian statistics, where the constant skewness of $\partial u_r/\partial r$ implies that the other higher absolute moments increase with the Taylor-scale Reynolds number.

5. The developed energy spectrums, calculated with the proposed closure of the von Kármán-Howarth equation, agrees quite well with the Kolmogorov law $\kappa^{-5/3}$ in a given interval of κ which defines the inertial subrange of Kolmogorov.

6. For developed energy spectrums, the Kolmogorov function is about constant in a wide range of separation distances and its maximum is quite close to 4/5, whereas the Kolmogorov constant is about equal to 1.93. As the consequence, the maximal finite scale Lyapunov exponent and the diffusivity coefficient, vary according to the Richardson law when the separation distance is of the order of the Taylor scale.

7. The proposed theory also describes very well the multifractality of the velocity difference, in the sense that, for developed energy spectrum, the scaling exponents of the longitudinal velocity difference, when expressed in terms of the moments order, exhibit the characteric shape observed by the various authors.

IX. ACKNOWLEDGMENTS

This work was partially supported by the Italian Ministry for the Universities and Scientific and Technological Research (MIUR).

X. APPENDIX

The von Kármán-Howarth equation gives the evolution in time of the longitudinal correlation function for isotropic turbulence. The correlation function of the velocity components is the symmetrical second order tensor $R_{ij}(\mathbf{r}) = \left\langle u_i u'_j \right\rangle$, where u_i and u'_j are the velocity components at $\mathbf{x}$ and $\mathbf{x}+\mathbf{r}$, respectively, being $\mathbf{r}$ the separation vector. The equations for R_{ij} are obtained by the Navier-Stokes equations written in the two points $\mathbf{x}$ and $\mathbf{x}+\mathbf{r}$ [6, 7]. For isotropic turbulence R_{ij} can be expressed as

$$R_{ij}(\mathbf{r}) = u^2 \left[(f-g)\frac{r_i r_j}{r^2} + g\delta_{ij} \right] \tag{58}$$

f and g are, respectively, longitudinal and lateral correlation functions, which are

$$f(r) = \frac{\langle u_r(\mathbf{x}) u_r(\mathbf{x}+\mathbf{r}) \rangle}{u^2},\ g(r) = \frac{\langle u_n(\mathbf{r}) u_n(\mathbf{x}+\mathbf{r}) \rangle}{u^2} \tag{59}$$

where u_r and u_n are, respectively, the velocity components parallel and normal to $\mathbf{r}$, whereas $r = |\mathbf{r}|$ and $u^2 = \langle u_r^2 \rangle = \langle u_n^2 \rangle = 1/3 \langle u_i u_i \rangle$. Due to the continuity equation, f and g are linked each other by the relationship

$$g = f + \frac{1}{2}\frac{\partial f}{\partial r} r \tag{60}$$

The von Kármán-Howarth equation reads as follows [6, 7]

$$\frac{\partial u^2 f}{\partial t} = K + 2\nu u^2 \left(\frac{\partial^2 f}{\partial r^2} + \frac{4}{r}\frac{\partial f}{\partial r} \right) \tag{61}$$

where K is an even function of r, which is defined by the following equation [6, 7]

$$\left(r\frac{\partial}{\partial r} + 3 \right) K(r) = \frac{\partial}{\partial r_k} \left\langle u_i u_i' (u_k - u_k') \right\rangle \tag{62}$$

and which can also be expressed as

$$K(r) = u^3 \left(\frac{\partial}{\partial r} + \frac{4}{r} \right) k(r) \tag{63}$$

where k is the longitudinal triple correlation function

$$k(r) = \frac{\left\langle u_r^2(\mathbf{x}) u_r(\mathbf{x}+\mathbf{r}) \right\rangle}{u^3} \tag{64}$$

The boundary conditions of Eq. (61) are [6, 7]

$$f(0) = 1, \quad \lim_{r\to\infty} f(r) = 0 \tag{65}$$

The viscosity is responsible for the decay of the turbulent kinetic energy, the rate of which is obtained putting $r = 0$ in the von Kármán-Howarth equation, i.e.

$$\frac{\partial u^2}{\partial t} = 10\nu u^2 \frac{\partial^2 f}{\partial r^2}(0) \tag{66}$$

This energy is distributed at different wave-lengths according to the energy spectrum $E(\kappa)$ which is calculated as the Fourier Transform of fu^2, whereas the "transfer function" $T(\kappa)$ is the Fourier Transform of K [7], i.e.

$$\begin{bmatrix} E(\kappa) \\ \\ T(\kappa) \end{bmatrix} = \frac{1}{\pi} \int_0^\infty \begin{bmatrix} u^2 f(r) \\ \\ K(r) \end{bmatrix} \kappa^2 r^2 \left(\frac{\sin \kappa r}{\kappa r} - \cos \kappa r \right) dr \tag{67}$$

where $\kappa = |\boldsymbol{\kappa}|$ and $T(\kappa)$ identically satisfies to the integral condition

$$\int_0^\infty T(\kappa) d\kappa = 0 \tag{68}$$

which states that K does not modify the total kinetic energy. The rate of energy dissipation ε is calculated for isotropic turbulence as follows [7]

$$\varepsilon = -\frac{3}{2}\frac{\partial u^2}{\partial t} = 2\nu \int_0^\infty \kappa^2 E(\kappa) d\kappa \tag{69}$$

The microscales of Taylor λ_T, and of Kolmogorov ℓ, are defined as

$$\lambda_T^2 = \frac{u^2}{\langle(\partial u_r/\partial r)^2\rangle} = -\frac{1}{\partial^2 f/\partial r^2(0)},\ \ell = \left(\frac{\nu^3}{\varepsilon}\right)^{1/4} \tag{70}$$

---

[1] Landau, L. D., 1944. *Fluid Mechanics*. Pergamon London, England, 1959.

[2] Ottino J. M., Mixing, Chaotic Advection, and Turbulence., *Annu. Rev. Fluid Mech.* **22**, 207–253, 1990.

[3] Truesdell, C. *A First Course in Rational Continuum Mechanics*, Academic, New York, 1977.

[4] Richardson, L. F, Atmospheric Diffusion shown on a distance-neighbour graph., *Proc. Roy. Soc. London*, A **110**, 709, 1926.

[5] Kolmogorov, A. N., Dissipation of Energy in Locally Isotropic Turbulence. Dokl. Akad. Nauk SSSR **32**, 1, 19-21, 1941.

[6] von Kármán, T. & Howarth, L., On the Statistical Theory of Isotropic Turbulence., *Proc. Roy. Soc.* A, **164**, 14, 192, 1938.

[7] Batchelor G.K., *The Theory of Homogeneous Turbulence*. Cambridge University Press, Cambridge, 1953.

[8] Guckenheimer J., Holmes P., *Nonlinear Oscillations, Dynamical Systems, and Bifurcations of Vector Fields*. Springer, 1990.

[9] Kuznetsov Y.A., *Elements of Applied Bifurcation Theory*. Springer, 2004.

[10] Prigogine I., *Time, Chaos and the Laws of Chaos*. Ed. Progress, Moscow, 1994.

[11] Feigenbaum M. J., *J. Stat. Phys.* **19**, 1978.

[12] Ruelle, D. & Takens, F., *Commun. Math Phys.* **20**, 167, 1971.

[13] Pomeau Y., Manneville P., *Commun Math. Phys.* **74**, 189, 1980.

[14] Eckmann J.P., Roads to turbulence in dissipative dynamical systems *Rev. Mod. Phys.* **53**, 643 - 654, 1981.

[15] Gollub, J.P. & Swinney, H.L. 1975. Onset of Turbulence in Rotating Fluid., *Physical Review Letters* **35**, 14, 927–930.

[16] Giglio, M., Musazzi S., & Perini, U. 1981. Transition to chaotic behavior via a reproducible sequence of period-doubling bifurcation, *Physical Review Letters* **47**, 243–246.

[17] Maurer, J., Libchaber A., 1979. Rayleigh-Bénard Experiment in Liquid Helium; Frequency Locking and the onset of turbulence, *Journal de Physique Letters* **40**, L419–L423.

[18] Lamb, H. *Hydrodynamics*, Dover Publications, 1945.

[19] Christiansen F., Rugh H. H., Computing Lyapunov spectra with continuous Gram-Schmidt orthonormalization, *Nonlinearity*, Vol. 10, No. 5, 1997 , pp. 1063-1072.

[20] Ershov S. V., Potapov A. B., On the Concept of Stationary Lyapunov Basis., *Physica D*, **118**, 167–198, 1998.

[21] Sreenivasan K. R., Antonia R. A., The Phenomenology of Small-Scale Turbulence., *Annu. Rev. Fluid Mech.* **29**, 435–472, 1997.

[22] Tabeling P., Zocchi G., Belin F., Maurer J. Willaime H., Probability Density functions, Skewness, and Flatness in Large Reynolds Number Turbulence, *Physical Review E* **53**, no. 2, 1613–1621, 1996.

[23] Belin F., Maurer J. Willaime H., Tabeling P., Velocity Gradient Distributions in Fully Developed Turbulence: An Experimental Study, *Physics of Fluid* **9**, no. 12, 3843–3850, 1997.

[24] Lehmann E.L., *Elements of Large-sample Theory.* Springer, 1999.

[25] Madow W. G., Limiting Distributions of Quadratic and Bilinear Forms., *The Annals of Mathematical Statistics*, Vol. 11, No. 2, (Jun. 1940), 125–146, 1940.

[26] Hildebrand F.B., *Introduction to Numerical Analysis*, Dover Publications, 1987.

[27] Kolmogorov, A. N., Refinement of Previous Hypothesis Concerning the Local Structure of Turbulence in a Viscous Incompressible Fluid at High Reynolds Number, *J. Fluid Mech.* **12**, 82-85, 1962.

[28] She Z.S. and Leveque E., Universal scaling laws in fully developed turbulence, *Phys. Rev. Lett.* **72**, 336, 1994.

[29] Benzi, R., Biferale L., Paladin G., Vulpiani A., Vergassola M., Multifractality in the Statistics of the Velocity Gradients in Turbulence, *Phys. Rev. Lett.* **67**, 17 2299–2302, 1991.

[30] Pullin D., Saffman P., On the Lundgren Townsend model of turbulent fine structure, *Phys. Fluids*, A **5**, 1,126, 1993.